

4-1-2010

# Electronic Structure and Volume Effect on Thermoelectric Transport in P -Type Bi and Sb Tellurides

Minsik Park

Junghwan Song

Julia E. Medvedeva

*Missouri University of Science and Technology, juliaem@mst.edu*

Miyoung Kim

*et. al. For a complete list of authors, see [http://scholarsmine.mst.edu/phys\\_facwork/1500](http://scholarsmine.mst.edu/phys_facwork/1500)*Follow this and additional works at: [http://scholarsmine.mst.edu/phys\\_facwork](http://scholarsmine.mst.edu/phys_facwork)Part of the [Physics Commons](#)

## Recommended Citation

M. Park et al., "Electronic Structure and Volume Effect on Thermoelectric Transport in P -Type Bi and Sb Tellurides," *Physical Review B - Condensed Matter and Materials Physics*, vol. 81, no. 15, pp. 155211-1-155211-5, American Physical Society (APS), Apr 2010.  
The definitive version is available at <http://dx.doi.org/10.1103/PhysRevB.81.155211>

This Article - Journal is brought to you for free and open access by Scholars' Mine. It has been accepted for inclusion in Physics Faculty Research & Creative Works by an authorized administrator of Scholars' Mine. This work is protected by U. S. Copyright Law. Unauthorized use including reproduction for redistribution requires the permission of the copyright holder. For more information, please contact [scholarsmine@mst.edu](mailto:scholarsmine@mst.edu).

**Electronic structure and volume effect on thermoelectric transport in *p*-type Bi and Sb tellurides**Min Sik Park,<sup>1</sup> Jung-Hwan Song,<sup>2,\*</sup> Julia E. Medvedeva,<sup>1</sup> Miyoung Kim,<sup>3</sup> In Gee Kim,<sup>4</sup> and Arthur J. Freeman<sup>2</sup><sup>1</sup>*Department of Physics, Missouri University of Science and Technology, Rolla, Missouri 65409, USA*<sup>2</sup>*Department of Physics and Astronomy, Northwestern University, Evanston, Illinois 60208, USA*<sup>3</sup>*Division of Energy System Research, Ajou University, Suwon 443-749, Republic of Korea*<sup>4</sup>*Graduate Institute of Ferrous Technology, Pohang University of Science and Technology, Pohang 790-784, Republic of Korea*

(Received 21 July 2009; revised manuscript received 18 February 2010; published 20 April 2010)

Thermoelectric transport properties (Seebeck coefficient,  $S$ , and electrical conductivity,  $\sigma$ ) of *p*-type Bi and Sb tellurides are investigated using a first-principles all-electron density-functional approach. We demonstrate that the carrier concentration, band gap, and lattice constants have an important influence on the temperature behavior of  $S$  and that the volume expansion by 5.5% in  $\text{Sb}_2\text{Te}_3$  results in an increase in  $S$  by 33  $\mu\text{V}/\text{K}$  at 300 K. We argue that in addition to the electronic structure characteristics, the volume also affects the value of  $S$  and hence should be considered as an origin of the experimental observations that  $S$  can be enhanced by doping  $\text{Sb}_2\text{Te}_3$  with Bi (which has a larger ionic size) in Sb sites or by the deposition of thick  $\text{Bi}_2\text{Te}_3$  layers alternating with thinner  $\text{Sb}_2\text{Te}_3$  layers in a superlattice,  $\text{Bi}_2\text{Te}_3/\text{Sb}_2\text{Te}_3$ . We show that the optimal carrier concentration for the best power factor of  $\text{Bi}_2\text{Te}_3$  and  $\text{Sb}_2\text{Te}_3$  is approximately  $10^{19} \text{ cm}^{-3}$ .

DOI: [10.1103/PhysRevB.81.155211](https://doi.org/10.1103/PhysRevB.81.155211)

PACS number(s): 72.20.Pa, 72.80.Jc, 71.20.Nr

The development of highly efficient thermoelectric (TE) materials is important for refrigeration and energy generation and storage technologies. The efficiency of TE materials is represented by the figure of merit,  $ZT = S^2 \sigma T / (\kappa_e + \kappa_L)$ , where  $S$  is the Seebeck coefficient,  $\sigma$  is the electrical conductivity, and  $\kappa_e$  and  $\kappa_L$  are the electronic and lattice thermal conductivities, respectively. Thus, a higher  $ZT$  can be obtained by decreasing the denominator (smaller  $\kappa_e$  and/or  $\kappa_L$ ) or by increasing the numerator (larger  $S$  and/or  $\sigma$ ).<sup>1,2</sup> Although the thermoelectric materials have been extensively studied for the last decade, there are only a few theoretical simulations of their transport properties.<sup>3,4</sup>

$\text{Bi}_2\text{Te}_3$  alloys with peak  $ZT \sim 1.0$  are well-known conventional materials for thermoelectric applications near room temperature.<sup>5</sup> In the experiments for  $\text{Bi}_2\text{Te}_3$  and  $\text{Sb}_2\text{Te}_3$ -based alloys, the doping of bismuth and antimony atoms in  $\text{Sb}_2\text{Te}_3$  and  $\text{Bi}_2\text{Te}_3$ , respectively, influences the thermoelectric properties,<sup>6–8</sup> where it is generally known that the antisite defects are the origin of the current carriers.<sup>9–11</sup> In addition, recently, the highest  $ZT$  value of  $\sim 2.4$  was reported at 300 K in *p*-type  $\text{Bi}_2\text{Te}_3/\text{Sb}_2\text{Te}_3$  superlattices.<sup>12</sup> Even though the phonon-blocking/electron-transmitting mechanism in the superlattice was suggested,<sup>12</sup> to our knowledge, the influence of the thickness and volume of each layer for the electronic transport coefficients of  $S$  and  $\sigma$  is not well understood. In this work, we first investigate the temperature-dependent behavior of the thermoelectric property in bulk  $\text{Bi}_2\text{Te}_3$ ,  $(\text{Bi}_{0.5}\text{Sb}_{0.5})_2\text{Te}_3$ , and  $\text{Sb}_2\text{Te}_3$ ; discuss the role of carrier concentration, band gap, and electronic structure; and compare the results to experiments. Second, we suggest that the dopant size effect by Bi and Sb cation doping can be one of the origins to influence the thermoelectric property, even though both Bi and Sb have the same number of valence electrons, and it is demonstrated that  $S$  in  $\text{Sb}_2\text{Te}_3$  increases due to the volume expansion associated with the doping of larger Bi atoms.

For the study, we considered the rhombohedral structure for  $\text{Bi}_2\text{Te}_3$  and  $\text{Sb}_2\text{Te}_3$ , and the hexagonal supercell structure<sup>13</sup> for  $(\text{Bi}_{0.5}\text{Sb}_{0.5})_2\text{Te}_3$  where each

Bi (Sb) atom has four and two nearest neighbors of Sb (Bi) and Bi (Sb), respectively, in the hexagonal plane. We used experimental lattice constants for  $\text{Bi}_2\text{Te}_3$  ( $a_{\text{BT}} = 4.386 \text{ \AA}$ ,  $c_{\text{BT}} = 30.497 \text{ \AA}$ ) and  $\text{Sb}_2\text{Te}_3$  ( $a_{\text{ST}} = 4.264 \text{ \AA}$ ,  $c_{\text{ST}} = 30.458 \text{ \AA}$ ),<sup>14,15</sup> and average lattice constants for  $(\text{Bi}_{0.5}\text{Sb}_{0.5})_2\text{Te}_3$ . The internal atomic positions in  $(\text{Bi}_{0.5}\text{Sb}_{0.5})_2\text{Te}_3$ ,  $\text{Bi}_2\text{Te}_3$ , and  $\text{Sb}_2\text{Te}_3$  were optimized via force and total-energy minimization.<sup>16,17</sup> Experimentally, the Sb-doped  $\text{Bi}_2\text{Te}_3$  shows *p*-type character;<sup>6–8</sup> therefore, we discuss only *p*-type Bi and Sb tellurides for comparing with experimental results. The electronic structure was calculated using the highly precise all-electron full-potential linearized augmented plane-wave (FLAPW) method in the local-density approximation (LDA) with spin-orbit coupling (SOC) included by a second variational method.<sup>16,17</sup> Further, the screened-exchange LDA (sX-LDA) method is used for obtaining correct band gaps at zero temperature. The sX-LDA method is known to provide a better description of the excited states and band gaps; in particular, good agreement with the experimental band gap (0.162 eV) was obtained for  $\text{Bi}_2\text{Te}_3$  (0.154 eV).<sup>18</sup> To determine the Seebeck coefficient and the electrical conductivity, we employed the distribution function given by Boltzmann's equation in the constant relaxation-time approximation.<sup>19</sup> For the calculation of the group velocity, which is included in the transport coefficients, we use full intraband optical matrix elements defined within the FLAPW method. The thermoelectric transport coefficients of  $S$  and  $\sigma$  can, therefore, be calculated as

$$\mathbf{L}_{\alpha,\beta}^{(\nu)} = e^2 \tau \int \frac{d\epsilon d\mathbf{k}}{8\pi^3} \left( -\frac{\partial f_0}{\partial \epsilon} \right) (\epsilon - \mu)^\nu \delta(\epsilon - \epsilon_{\mathbf{k}}) \mathbf{v}_{\mathbf{k}}^\alpha \mathbf{v}_{\mathbf{k}}^\beta, \quad (1)$$

$$\boldsymbol{\sigma} = \mathbf{L}^{(0)}, \quad \mathbf{S} = -\frac{1}{eT} (\mathbf{L}^{(0)})^{-1} \mathbf{L}^{(1)}, \quad (2)$$

where  $\tau$ ,  $f_0$ , and  $\mathbf{v}_{\mathbf{k}}$  denote the relaxation time, Fermi-Dirac distribution function, and group velocity, respectively;  $e$  denotes the electrical charge;  $\mu$  the chemical potential;  $T$  the

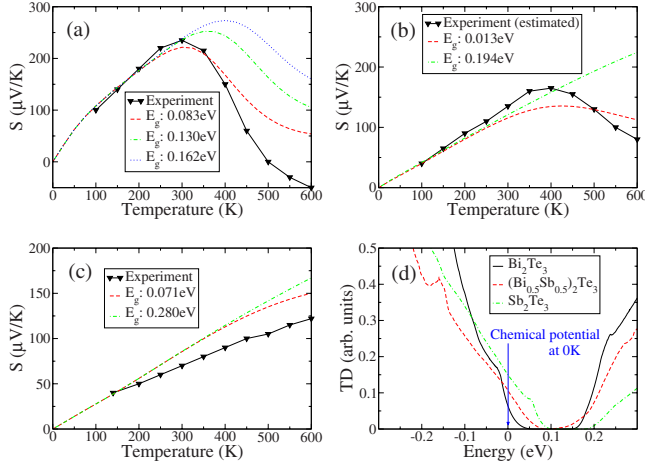


FIG. 1. (Color online) Temperature-dependent Seebeck coefficients of (a)  $\text{Bi}_2\text{Te}_3$  at the carrier density of  $1.32 \times 10^{19} \text{ cm}^{-3}$ , (b)  $(\text{Bi}_{0.5}\text{Sb}_{0.5})_2\text{Te}_3$  at  $3.16 \times 10^{19} \text{ cm}^{-3}$ , and (c)  $\text{Sb}_2\text{Te}_3$  at  $8.70 \times 10^{19} \text{ cm}^{-3}$ , where the experimental data are adapted from Ref. 6; and (d) the TDs defined by Eq. (1) for the cases with the band gap from the SOC-LDA.

temperature; and  $\delta(\varepsilon - \varepsilon_{\mathbf{k}})$  the Dirac delta function. Different carrier concentration was treated within the rigid-band model<sup>20</sup> and a scissor operator<sup>21</sup> is applied to obtain the experimental band gaps in the transport coefficient calculations.

In previous experimental work, the thermoelectric properties of  $p$ -type  $(\text{Bi}_{1-x}\text{Sb}_x)_2\text{Te}_3$  ( $x=0.00, 0.33, 0.39, 0.66, 0.71$ , and  $1.00$ ) were studied systematically.<sup>6</sup> Hence, for comparing with the experimental results, we have calculated  $S$  and  $\sigma$  for three  $p$ -type materials,  $\text{Bi}_2\text{Te}_3$ ,  $(\text{Bi}_{0.5}\text{Sb}_{0.5})_2\text{Te}_3$ , and  $\text{Sb}_2\text{Te}_3$ , using a rigid-band shift that corresponds to the experimental carrier densities. Figure 1(a) shows three calculated Seebeck coefficients<sup>22</sup> of  $\text{Bi}_2\text{Te}_3$  with the different band gaps at the experimental carrier density of  $1.32 \times 10^{19} \text{ cm}^{-3}$  compared with experimental data. We here simulated the Seebeck coefficients with three different band gaps, i.e.,  $0.083 \text{ eV}$  (SOC-LDA),  $0.162 \text{ eV}$  (extrapolated to  $0 \text{ K}$  from the measured values),<sup>23</sup> and  $0.130 \text{ eV}$  (measured at room temperature).<sup>24</sup> Below  $300 \text{ K}$ , all calculated results show excellent agreement with experiment, that is, a monotonic increase in  $S$  with temperature, which can be attributed to the very narrow energy window from the Fermi-Dirac statistics. Above  $300 \text{ K}$ , the overall Seebeck results show similar behavior to experiment; the different band gaps yield different  $S$ , and different peak temperatures at which a maximal peak of  $S$  appears, which is due to the compensated  $p$ -type contribution to Seebeck by thermally excited  $n$ -type carriers across the band gap. Thus, a larger band gap induces a higher peak temperature. The rapid decrease in  $S(T)$  in the experiment compared to our results may be attributed to the band-gap reduction<sup>24</sup> and to dominant  $n$ -type defect creation at high temperatures.<sup>10</sup>

The  $50\%$  Sb-doped  $\text{Bi}_2\text{Te}_3$  shows similar behavior to the  $\text{Bi}_2\text{Te}_3$  case at low temperatures for the temperature dependent  $S$  in the experiment [Figs. 1(a) and 1(b)]. However, the peak shifts to a higher temperature (near  $400 \text{ K}$ ) while the highest  $S$  value ( $170 \mu\text{V/K}$ ) is lower—as compared to

$\text{Bi}_2\text{Te}_3$ . In this case, the experimental carrier density of  $3.16 \times 10^{19} \text{ cm}^{-3}$ , which is higher than that in  $\text{Bi}_2\text{Te}_3$ , is used. Since the experimental band gap is unknown for this composition, we used the sX-LDA method to obtain the correct band gap at zero temperature— $0.194 \text{ eV}$ , for  $(\text{Bi}_{0.5}\text{Sb}_{0.5})_2\text{Te}_3$ , which is between the experimental band gaps of  $0.162 \text{ eV}$  ( $\text{Bi}_2\text{Te}_3$ ) and  $0.280 \text{ eV}$  ( $\text{Sb}_2\text{Te}_3$ ).<sup>23,25</sup> We found that  $S(T)$  with the sX-LDA band gap at low temperatures (below  $400 \text{ K}$ ) is closer to the experimental one than that with the SOC-LDA band gap ( $0.013 \text{ eV}$ ). For  $\text{Sb}_2\text{Te}_3$ , the experimental carrier density of  $8.70 \times 10^{19} \text{ cm}^{-3}$  is used. In Fig. 1(c), two calculated  $S$ 's, in which the band gap of  $0.071 \text{ eV}$  (SOC-LDA) and  $0.280 \text{ eV}$  (experiment)<sup>25</sup> are used, are compared to the experimental value. Even though there is a difference between the  $S$  values of experiment and calculations, the trend in  $S(T)$  up to  $600 \text{ K}$  is similar. The monotonically increasing behavior of  $S$  without the maximal peak comes from the large carrier density rather than the large band gap because the smaller band gap of  $0.071 \text{ eV}$  (SOC-LDA) also shows the increase in  $S$  instead of showing a peak near room temperature, as in  $\text{Bi}_2\text{Te}_3$ . This is also why the band gap has little effect on  $S$  in this simulation and yields very similar results for  $S$  between the two different band gaps,  $0.071$  and  $0.280 \text{ eV}$ .

To analyze the behavior of  $S(T)$ , we have calculated the transport distribution (TD),<sup>3,4</sup> which includes all necessary information, such as the group velocities and density of states,

$$\text{TD}_{\alpha,\beta}(\varepsilon) = \int d\mathbf{k} v_{\mathbf{k}}^{\alpha} v_{\mathbf{k}}^{\beta} \delta(\varepsilon - \varepsilon_{\mathbf{k}}). \quad (3)$$

Here, the larger asymmetric TD below and above the chemical potential (i.e., a larger slope at the chemical potential) yields larger  $S$ . In Fig. 1(d), the transport distributions in three materials are plotted with respect to  $\mu(0)$  and the chemical potential at  $0 \text{ K}$ . In  $\text{Sb}_2\text{Te}_3$ , the position of  $\mu(0)$  is the furthest away from the valence-band maximum (VBM) compared to  $\text{Bi}_2\text{Te}_3$  and  $(\text{Bi}_{0.5}\text{Sb}_{0.5})_2\text{Te}_3$  because of its highest carrier density. This deep chemical potential in  $\text{Sb}_2\text{Te}_3$  causes the highest peak temperature of  $S$  compared to  $(\text{Bi}_{0.5}\text{Sb}_{0.5})_2\text{Te}_3$  and  $\text{Bi}_2\text{Te}_3$ . In addition, the largest TD, highest conductivity, yields the smallest  $S(T)$  in  $\text{Sb}_2\text{Te}_3$ . Also, the overall steepest slope near the VBM of  $\text{Bi}_2\text{Te}_3$  suggests that larger  $S$  in  $\text{Bi}_2\text{Te}_3$  compared to  $(\text{Bi}_{0.5}\text{Sb}_{0.5})_2\text{Te}_3$  and  $\text{Sb}_2\text{Te}_3$  is partially due to the electronic structure differences as discussed below.

Figure 2(a) shows a comparison of the calculated  $S$  with experiment for all materials considered for various concentrations at  $300 \text{ K}$ . The theoretical results are in good agreement with experiment. The decrease in  $S$  as the carrier concentration increases, follows the general behavior of  $S$  in semiconductors. The carrier dependence of  $\sigma$  in Fig. 2(b) also shows usual behavior, that is, an increase in  $\sigma$  as the carrier concentration increases. Here, the constant relaxation-time ( $\tau$ ) value of  $1.0 \times 10^{-14} \text{ s}$  is used. From the comparison between the theoretical and the experimental values, we can then fit  $\tau$ 's at  $300 \text{ K}$  to obtain  $0.59 \times 10^{-14}$ ,  $0.81 \times 10^{-14}$ , and  $2.16 \times 10^{-14} \text{ s}$  for  $\text{Bi}_2\text{Te}_3$ ,  $(\text{Bi}_{0.5}\text{Sb}_{0.5})_2\text{Te}_3$ , and  $\text{Sb}_2\text{Te}_3$ , re-

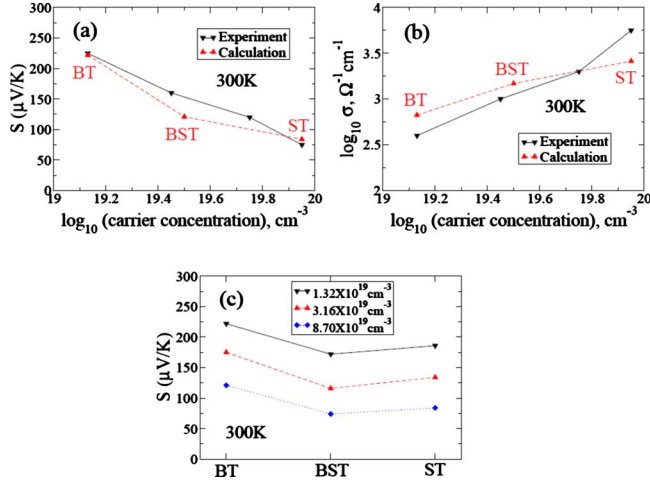


FIG. 2. (Color online) Carrier concentration dependent (a) Seebeck coefficients and (b) conductivities from the calculations for  $\text{Bi}_2\text{Te}_3$  (BT),  $(\text{Bi}_{0.5}\text{Sb}_{0.5})_2\text{Te}_3$  (BST), and  $\text{Sb}_2\text{Te}_3$  (ST), and the experiment (adapted from Ref. 6); and (c) compound dependent Seebeck coefficients for each with the same carrier concentration.

spectively, all of which have the same typical order of the previously assumed value,  $10^{-14}$  s.<sup>4</sup> These fitted values also indicate a possible dramatic increase in the electronic contribution to the thermal conductivity when the Sb doping concentration becomes larger in  $\text{Bi}_2\text{Te}_3$ . Experimentally, the thermal conductivity of  $\text{Bi}_2\text{Te}_3$  at 300 K does not change much, up to 75% Sb doping ( $1.5\text{--}2\text{ W m}^{-1}\text{ K}^{-1}$ ).<sup>6</sup> On the contrary,  $\text{Bi}_2\text{Te}_3$  with Sb doping larger than 75% shows a large increase in  $\kappa$  ( $2\text{--}4.5\text{ W m}^{-1}\text{ K}^{-1}$ ). Hence, the relaxation-time values fitted for three different compositions above appear to have a correlation with the sharp increase in  $\kappa$  in the experiments. Due to this composition dependence of the relaxation time, we expect that the main contribution to the change in  $ZT$  for the variation in Sb doping concentration  $<75\%$  is the power factor defined by  $S^2\sigma$ . To see the electronic structure effect for  $S$ , the  $S$ 's are plotted at the same carrier concentrations for each compound in Fig. 2(c). The  $S$ 's curves of  $(\text{Bi}_{0.5}\text{Sb}_{0.5})_2\text{Te}_3$  and  $\text{Sb}_2\text{Te}_3$  are similar and lower than  $\text{Bi}_2\text{Te}_3$  that originates from the different contribution of electronic structure between  $\text{Bi}_2\text{Te}_3$  and  $(\text{Bi}_{0.5}\text{Sb}_{0.5})_2\text{Te}_3$ ,  $\text{Sb}_2\text{Te}_3$ , i.e., the different slopes between their TD's as seen in Fig. 1(d). However, it is difficult to explain the  $S$  behavior by the simple comparison between the band structures along high-symmetry lines such as counting the peaks near the VBM in Fig. 3. In fact, the band edges of these materials have been studied thoroughly and their VBMs are not located along the high-symmetry lines.<sup>26,27</sup>

As one of the possible origins for the change in the thermoelectric transport property by substitutional doping, the volume effect is investigated. Since the volume may change between  $\text{Bi}_2\text{Te}_3$  (the higher limit) and  $\text{Sb}_2\text{Te}_3$  (the lower limit) by the doping, we calculated the  $S$ 's shown in Figs. 4(a) and 4(b) with three different lattice constants, namely,  $(a_{\text{BT}}, c_{\text{BT}})$ ,  $[a_{\text{ave}}=(a_{\text{BT}}+a_{\text{ST}})/2, c_{\text{ave}}=(c_{\text{BT}}+c_{\text{ST}})/2]$ , and  $(a_{\text{ST}}, c_{\text{ST}})$ . The carrier concentration was kept constant and equal to  $1.32 \times 10^{19}\text{ cm}^{-3}$  for comparison of the different lattice parameters and the experimental band gaps were used for  $\text{Bi}_2\text{Te}_3$  and  $\text{Sb}_2\text{Te}_3$ .

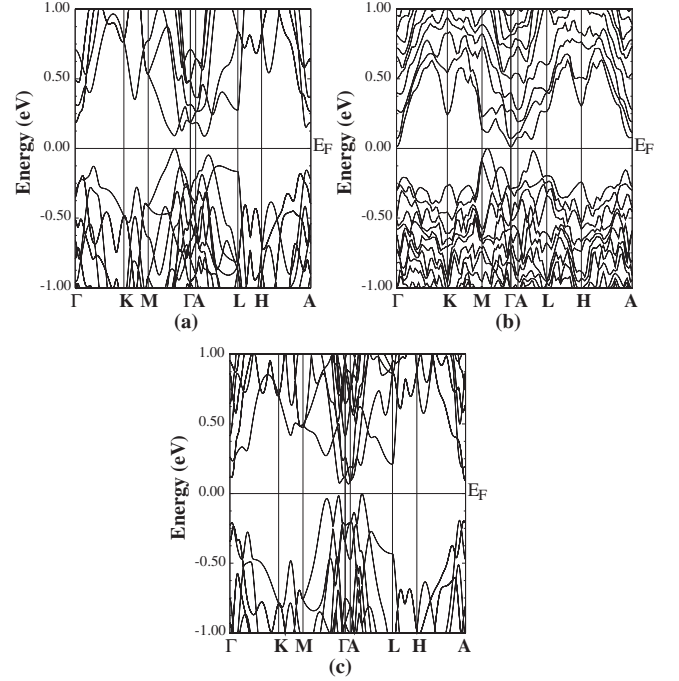


FIG. 3. Band structures of the hexagonal (a)  $\text{Bi}_2\text{Te}_3$ , (b)  $(\text{Bi}_{0.5}\text{Sb}_{0.5})_2\text{Te}_3$ , and (c)  $\text{Sb}_2\text{Te}_3$  in the SOC-LDA.

In  $\text{Sb}_2\text{Te}_3$ , with the increase in volume by 5.5% (from  $V_{\text{ST}}$  to  $V_{\text{BT}}$ ),  $S$  increases by about  $33\text{ }\mu\text{V/K}$  at 300 K, and the peak temperature with the highest  $S$  decreases from 575 to

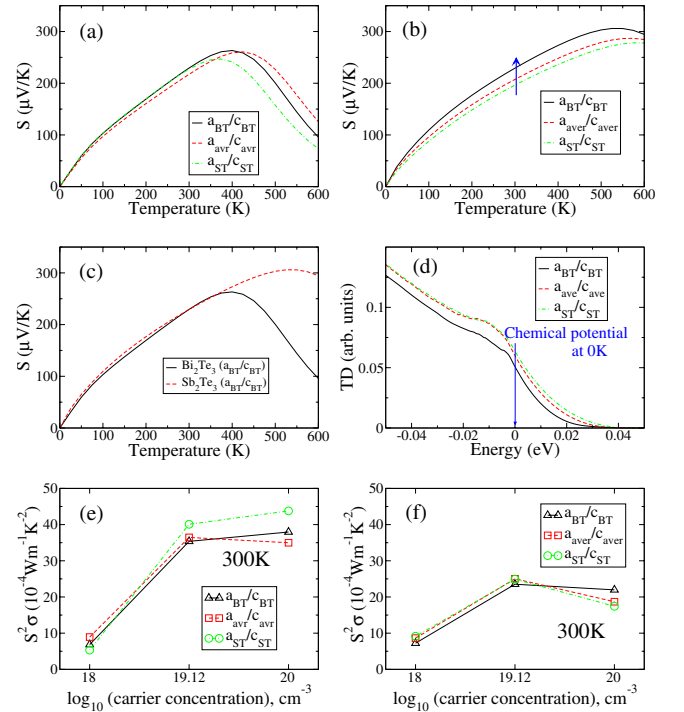


FIG. 4. (Color online) Temperature-dependent Seebeck coefficients at the carrier density of  $1.32 \times 10^{19}\text{ cm}^{-3}$  of (a)  $\text{Bi}_2\text{Te}_3$  and (b)  $\text{Sb}_2\text{Te}_3$  with lattice constants  $a_{\text{BT}}/c_{\text{BT}}$ ,  $a_{\text{ave}}/c_{\text{ave}}$ , and  $a_{\text{ST}}/c_{\text{ST}}$ ; and of (c)  $\text{Bi}_2\text{Te}_3$  and  $\text{Sb}_2\text{Te}_3$  with the same lattice constant of  $a_{\text{BT}}/c_{\text{BT}}$ ; and (d) TD's for the cases in Fig. 4(b); and carrier concentration dependent power factors at each lattice constant of (e)  $\text{Bi}_2\text{Te}_3$  and (f)  $\text{Sb}_2\text{Te}_3$ .



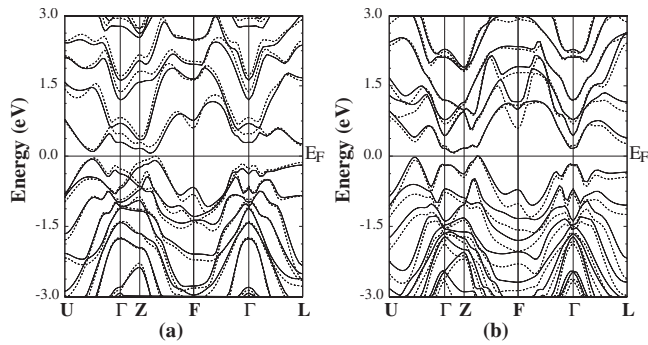


FIG. 5. Band structures of the rhombohedral (a)  $\text{Bi}_2\text{Te}_3$  and (b)  $\text{Sb}_2\text{Te}_3$  with lattice constants  $a_{\text{BT}}/c_{\text{BT}}$  (solid line) and  $a_{\text{ST}}/c_{\text{ST}}$  (dotted line) in the SOC-LDA.

525 K in Fig. 4(b). One can expect that the volume increase causes “a larger number of carriers per unit cell” and thus a deeper chemical potential. Then if the electronic structure remains the same, this should decrease  $S$  and induce a larger peak temperature, as explained above. However, our calculations show the opposite results for which, as we shall see, the TD distortion at the chemical potential can be account for.

Now, the increased bond length between atoms reduces hybridization, which gives rise to a narrower band dispersion as in Fig. 5(b) and high effective masses, and thus induces the smaller TD values as in Fig. 4(d). The effect in the electronic structure by the enlarged volume overcompensates the effect of a larger number of carriers/unit cell and results in a shallower chemical potential (a lower peak temperature) and a larger  $S$ . From Fig. 4(c), in the comparison of  $S$  for  $\text{Bi}_2\text{Te}_3$  and  $\text{Sb}_2\text{Te}_3$  with the same volume of  $V_{\text{BT}}$ , we see that  $\text{Sb}_2\text{Te}_3$  exhibits a similar or even slightly higher  $S$  than that of  $\text{Bi}_2\text{Te}_3$ , which indicates that the volume effect is an important factor rather than different band structures to determine  $S$  in this same carrier concentration.

In the  $V_{\text{avr}}$  case of  $\text{Bi}_2\text{Te}_3$ , the volume reduction results in a lowering of  $S$  by  $13 \mu\text{V}/\text{K}$  at 300 K and the shift of peak temperature from 400 to 425 K [Fig. 4(a)], which can be understood in the same way as with the above  $\text{Sb}_2\text{Te}_3$  case. However, in  $\text{Bi}_2\text{Te}_3$  case, the volume reduction by a smaller  $V_{\text{ST}}$  shows different results. In this case, the volume reduction shows  $S$  to be similar to the  $V_{\text{BT}}$  case at 300 K [Fig. 4(a)]. Compared to other volume changed cases, the relaxation effect of atomic positions in this case is largest and distinct from other cases.<sup>28</sup> Different from the band narrowing in the volume-dependent  $\text{Sb}_2\text{Te}_3$  cases, this large relaxation shifts the highest valence band slightly up [compared to the previous VBM (along U- $\Gamma$ ) in the  $V_{\text{BT}}$  case] especially, along  $\Gamma$ -Z, Z-F, and  $\Gamma$ -L symmetry lines, in addition to the broader band dispersion [Fig. 5(a)]. Hence, in the case of the smaller volume effect in  $\text{Bi}_2\text{Te}_3$ , due to its large atomic relaxation effect, band structures should be carefully investi-

gated instead of simply applying band broadening analysis, compared to the larger volume effect.<sup>29</sup>

Therefore, the volume effect can be an important part of an origin of the results that Bi doped into bulk  $\text{Sb}_2\text{Te}_3$  or a deposition of thick layers of  $\text{Bi}_2\text{Te}_3$  alternating with thinner layers of  $\text{Sb}_2\text{Te}_3$ , i.e., superlattices of  $\text{Bi}_2\text{Te}_3/\text{Sb}_2\text{Te}_3$  can improve  $S$ , although they reduce  $\sigma$ . On the contrary, Sb doped into bulk  $\text{Bi}_2\text{Te}_3$  or thick  $\text{Sb}_2\text{Te}_3$  layers would contribute to a lower  $S$  but a higher  $\sigma$ . In addition, to improve  $S$  of bulk  $\text{Sb}_2\text{Te}_3$ , we can consider the inclusion of nanodots with a larger band gap, which does not affect the VBM of  $\text{Sb}_2\text{Te}_3$  and a larger lattice constant compared to those of bulk  $\text{Sb}_2\text{Te}_3$ .

Thus, for enhancing the power factor (PF), an optimized Sb doping ratio in bulk  $\text{Bi}_2\text{Te}_3$  or the thickness of  $\text{Bi}_2\text{Te}_3$  layers in superlattices should be carefully controlled. To see this, the volume dependent PFs at 300 K were calculated at the different carrier concentrations of  $10^{18}$ ,  $1.32 \times 10^{19}$ , and  $10^{20} \text{ cm}^{-3}$ , where we used the constant relaxation time of  $10^{-14} \text{ s}$  for the calculation of  $\sigma$  in all cases. In bulk  $\text{Bi}_2\text{Te}_3$ , from Fig. 4(e), the smaller volume shows better PF especially at high carrier concentrations ( $>10^{19} \text{ cm}^{-3}$ ). In this case, the effect of the volume change on the PF at the low carrier concentration of  $10^{18} \text{ cm}^{-3}$  is mainly manifested by  $S$  rather than  $\sigma$ . However, the PF at high carrier concentrations is improved mainly by  $\sigma$  through the volume reduction. In bulk  $\text{Sb}_2\text{Te}_3$ , from Fig. 4(f), the volume effect on the PF is much smaller compared to the  $\text{Bi}_2\text{Te}_3$  case and the larger volume shows better PF at the high carrier concentration of  $10^{20} \text{ cm}^{-3}$ . Contrary to the above bulk  $\text{Bi}_2\text{Te}_3$ , the effect of the volume change on the PF at the low carrier concentrations of  $10^{18}$  and  $1.32 \times 10^{19} \text{ cm}^{-3}$  is mainly shown by  $\sigma$  but, at the high carrier concentration of  $10^{20} \text{ cm}^{-3}$ , it is mainly shown by  $S$ . Considering the decrease in the relaxation time at the larger carrier concentration, both the  $\text{Bi}_2\text{Te}_3$  and  $\text{Sb}_2\text{Te}_3$  appear to show the optimal carrier concentration of approximately  $10^{19} \text{ cm}^{-3}$ .

In summary, using a first-principles density-functional approach, we have calculated the transport coefficients for pure and mixed Bi and Sb tellurides. We showed that the carrier concentration, electronic structure, and volume have an important influence on the temperature dependent  $S$ , such as the peak location and the slope. We found that the optimal carrier concentration for the best power factor of  $\text{Bi}_2\text{Te}_3$  and  $\text{Sb}_2\text{Te}_3$  is approximately  $10^{19} \text{ cm}^{-3}$ . This may give a good insight to fabricate more efficient thermoelectric materials and devices.

This work was supported by the Office of Naval Research (Grant No. ONR N00014-09-1-0733), the Korean Research Foundation Grant by MOEHRD (Grant No. KRF 2007-412-J04001), the Steel Innovation Program by POSCO, and the Petroleum Research Fund of the American Chemical Society (Grant No. 47491-610).

\*jhsong@pluto.phys.northwestern.edu

- <sup>1</sup>D.-Y. Chung, T. Hogan, P. Brazis, M. Rocci-Lane, C. Kannewurf, M. Bastea, C. Uher, and M. G. Kanatzidis, *Science* **287**, 1024 (2000).
- <sup>2</sup>T. M. Tritt and M. A. Subramanian, *MRS Bull.* **31**, 188 (2006).
- <sup>3</sup>G. D. Mahan and J. O. Sofo, *Proc. Natl. Acad. Sci. U.S.A.* **93**, 7436 (1996).
- <sup>4</sup>T. J. Scheidemantel, C. Ambrosch-Draxl, T. Thonhauser, J. V. Badding, and J. O. Sofo, *Phys. Rev. B* **68**, 125210 (2003).
- <sup>5</sup>G. J. Snyder and E. S. Toberer, *Nature Mater.* **7**, 105 (2008).
- <sup>6</sup>H. W. Jeon, H. P. Ha, D. B. Hyun, and J. D. Shim, *J. Phys. Chem. Solids* **52**, 579 (1991).
- <sup>7</sup>A. Giani, A. Boulouz, B. Aboulfarah, F. Pascal-Delannoy, A. Foucaran, A. Boyer, and A. Mzerd, *J. Cryst. Growth* **204**, 91 (1999).
- <sup>8</sup>J. Jiang, L. Chen, S. Bai, Q. Yao, and Q. Wang, *J. Cryst. Growth* **277**, 258 (2005).
- <sup>9</sup>C. B. Satterthwaite and R. W. Ure, Jr., *Phys. Rev.* **108**, 1164 (1957).
- <sup>10</sup>G. R. Miller and C. Li, *J. Phys. Chem. Solids* **26**, 173 (1965).
- <sup>11</sup>H. Iwasaki, A. Ohishi, T. Kajihara, and S. Sano, *Jpn. J. Appl. Phys., Part 1* **42**, 5477 (2003).
- <sup>12</sup>R. Venkatasubramanian, E. Siivola, T. Colpitts, and B. O'Quinn, *Nature (London)* **413**, 597 (2001).
- <sup>13</sup>P. Larson, S. D. Mahanti, and M. G. Kanatzidis, *Phys. Rev. B* **61**, 8162 (2000).
- <sup>14</sup>S. Nakajima, *J. Phys. Chem. Solids* **24**, 479 (1963).
- <sup>15</sup>T. L. Anderson and H. B. Krause, *Acta Crystallogr., Sect. B: Struct. Crystallogr. Cryst. Chem.* **30**, 1307 (1974).
- <sup>16</sup>E. Wimmer, H. Krakauer, M. Weinert, and A. J. Freeman, *Phys. Rev. B* **24**, 864 (1981).
- <sup>17</sup>H. J. F. Jansen and A. J. Freeman, *Phys. Rev. B* **30**, 561 (1984).
- <sup>18</sup>M. Kim, A. J. Freeman, and C. B. Geller, *Phys. Rev. B* **72**, 035205 (2005).
- <sup>19</sup>In Ref. 4, the calculated  $S$  and  $\sigma$  in the constant relaxation-time approximation show good agreement with experiment.
- <sup>20</sup>The rigid-band model used in this work can be considered in the point (antisite) defect limit. Thus the electronic structure is not changed significantly in this limit. However, the rigid-band model is not expected to work well at high concentrations of defects/impurities due to the possible interactions between them. Indeed, the rigid-band model is known to work well up to the carrier concentration of  $10^{20}$  cm<sup>-3</sup> (Ref. 4).
- <sup>21</sup>J. L. P. Hughes and J. E. Sipe, *Phys. Rev. B* **53**, 10751 (1996).
- <sup>22</sup>The Bi and Sb tellurides show anisotropy in  $S$  and  $\sigma$  between basal plane and trigonal axis ( $c$  direction) (Ref. 4). We used the calculated  $S$  in the  $ab$  plane for comparison with experimental data since the directions of electrical current are parallel to the (111) cleavage planes. (Ref. 6, and references therein).
- <sup>23</sup>B. M. Goltsman, B. A. Kudinov, and I. A. Smirnov, *Thermoelectric Semiconductor Material Based on Bi<sub>2</sub>Te<sub>3</sub>* (Army Foreign Science and Technology Center, Charlottesville, VA, 1973).
- <sup>24</sup>I. G. Austin, *Proc. Phys. Soc. London* **72**, 545 (1958).
- <sup>25</sup>*Numerical Data and Functional Relationships in Science and Technology*, Landolt-Börnstein, New Series, Group III Vol. 17, Pt. F, edited by O. Madelung, M. Schulz, and H. Weiss (Springer, New York, 1983).
- <sup>26</sup>S. J. Youn and A. J. Freeman, *Phys. Rev. B* **63**, 085112 (2001).
- <sup>27</sup>P. Larson, *Phys. Rev. B* **74**, 205113 (2006).
- <sup>28</sup>In the fixed structure, the calculated  $S$  is smaller than that of Bi<sub>2</sub>Te<sub>3</sub> with  $a_{ave}/c_{ave}$  due to the volume effect.
- <sup>29</sup>In Fig. 2(c), we can also see the similar behavior, where  $S$  of (Bi<sub>0.5</sub>Sb<sub>0.5</sub>)<sub>2</sub>Te<sub>3</sub> showing the large atomic relaxation is smaller than that of Sb<sub>2</sub>Te<sub>3</sub> at the same carrier density, even though the volume of (Bi<sub>0.5</sub>Sb<sub>0.5</sub>)<sub>2</sub>Te<sub>3</sub> is larger than that of Sb<sub>2</sub>Te<sub>3</sub>.